Computational Model Predicts Paracrine and Intracellular Drivers of Fibroblast Phenotype After Myocardial Infarction

Angela C. Zeigler[1], Anders R. Nelson[2,3], Anirudha S. Chandrabhatla[1], Olga Brazhkina[1,5],

Jeffrey W. Holmes[1,3,4], Jeffrey J. Saucerman[1,3,*]

[1]Department of Biomedical Engineering, University of Virginia, Charlottesville, VA, USA

[2]Department of Pharmacology, University of Virginia, Charlottesville, VA, USA

[3]Robert M. Berne Cardiovascular Research Center, University of Virginia, Charlottesville, VA, USA

[4]Department of Medicine, University of Virginia, Charlottesville, VA, USA

[5]Present Address: Coulter Department of Biomedical Engineering, Emory University, Atlanta, GA, USA

* Corresponding Author:

Dr. Jeffrey J. Saucerman

Department of Biomedical Engineering, University of Virginia

PO Box 800759

Charlottesville, VA 22908-0759

jsaucerman@virginia.edu

Abstract

The fibroblast is a key mediator of wound healing in the heart and other organs, yet how it integrates multiple time-dependent paracrine signals to control extracellular matrix synthesis has been difficult to study *in vivo*. Here, we extended a computational model to simulate the dynamics of fibroblast signaling and fibrosis after myocardial infarction in response to time-dependent data for nine paracrine stimuli. This computational model was validated against dynamic collagen expression and collagen area fraction data from post-infarction rat hearts. The model predicted that while many features of the fibroblast phenotype at inflammatory or maturation phases of healing could be recapitulated by single static paracrine stimuli (interleukin-1 and angiotensin-II, respectively), mimicking of the proliferative phase required paired stimuli (e.g. TGFβ and angiotensin-II). Virtual overexpression screens with static cytokine pairs and after myocardial infarction predicted phase-specific regulators of collagen expression. Several regulators increased (Smad3) or decreased (Smad7, protein kinase G) collagen expression specifically in the proliferative phase. NADPH oxidase overexpression sustained collagen expression from proliferative to maturation phases, driven by TGFβ and endothelin positive feedback loops. Interleukin-1 overexpression suppressed collagen via NFκB and BAMBI (BMP and activin membrane-bound inhibitor) incoherent feedforward loops, but it then later sustained collagen expression due to the TGFβ positive feedback loop. These model-based predictions reveal network mechanisms by which the dynamics of paracrine stimuli and interacting signaling pathways drive the progression of fibroblast phenotypes and fibrosis after myocardial infarction.

Introduction

45

46 Wound healing is a complex process that involves a dynamic interplay between

47 inflammatory and proliferative signaling. This process is especially important following

48 injury to the heart, where cardiomyocytes are unable to regenerate. Scar formation and

49 the preservation of viable heart muscle are important for continued cardiac function[1].

50 After myocardial infarction (MI), ACE inhibitors and beta blockers are prescribed to

51 prevent adverse cardiac remodeling and heart failure [2], but the risk of heart failure and

52 cardiac-related death post-MI remains high[3–5]. This is partly because wound healing is

53 a balancing act between clearance of debris and formation of new scar, and the regulators

54 of this dynamic process are not fully understood. Therefore, attempts to find therapeutic

55 targets that allow for adequate collagen expression while avoiding excessive fibrosis have

56 been largely unsuccessful. For example, although increased levels of interleukin-1 (IL1)

57 have been linked to fibrosis and diminished cardiac index post-MI[6], blocking IL1 post-

58 MI does not consistently improve healing and is actually associated with an increased

59 risk of secondary MI[7, 8].

60   Myocardial infarcts follow a healing process that is similar to that in other organs

61 [9, 10]. There is first an inflammatory phase characterized by extracellular matrix (ECM)

62 breakdown and myocyte necrosis, which lasts around 2 days in rats and 5 days in larger

63 mammals [11]. Then, the proliferative phase lasts around 2-5 days in rats (2 weeks in

64 large mammals), during which fibroblasts proliferate, migrate into the wound,

65 differentiate into myofibroblasts, and generate large amounts of collagen I and III and

66 other ECM proteins [11, 12]. Ultimately, the wound matures into a stable scar with

67 balanced ECM production and degradation. In the adult heart, cardiomyocytes do not

3

68   proliferate sufficiently to re-populate the wound, so the ultimate fate of cardiac tissue

69   depends on the behavior of cardiac fibroblasts. Excessive degradation can lead to

70   ventricular dilation and wall rupture due to the loss of structural integrity in the heart wall

71   [13]. Conversely, excessive ECM deposition, particularly in myocardium remote from

72   the infarct, can lead to diastolic dysfunction [14, 15]. Many patients with heart failure

73   post-MI have both dilation and fibrosis [1].

74   A beneficial infarct healing process likely involves a transient burst of collagen

75   deposition that replaces lost cardiomyocytes with strong ECM without a sustained

76   increase in ECM synthesis that leads to adverse remodeling [16]. This "transient fibrosis"

77   is likely facilitated by many different factors including inflammatory cell phenotype and

78   number, the pre-infarct signaling state, the size of the infarct, and the health of the

79   remaining cardiac vessels [17, 18]. Fibroblasts play a prominent role throughout the

80   entire wound healing process, and therefore present a good system for studying how cells

81   respond to the dynamic signaling environment of wound healing[19]. Additionally,

82   understanding how fibroblasts respond during the different phases of wound healing

83   could identify mechanisms by which fibrosis develops in other organs.

84   Myocardial infarct healing is notoriously difficult to investigate because it

85   involves many dynamic and interacting signaling processes. Fibroblasts are particularly

86   difficult to study *in situ* during wound healing because they can differentiate from many

87   different cell types and there is no clear consensus on fibroblast markers[20].

88   Computational modeling has been a useful method for investigating complex dynamic

89   processes in many areas of biology. Although models have been constructed to study the

90   wound healing process post-MI[21], no such model has yet been applied to study

91   fibroblast intracellular signaling and phenotypic changes during myocardial wound

92   healing[20, 22]. This study integrates a large-scale computational model of cardiac

93   fibroblast signaling [23] together with post-MI experimental data for nine time-dependent

94   paracrine stimuli to identify key paracrine and intracellular drivers of fibroblast

95   phenotype after MI. This computational model of post-MI fibroblast dynamics was

96   validated against independent experimental *in vivo* time courses of collagen mRNA and

97   collagen area fraction throughout infarct healing. Next, we applied the computational

98   model to identify simpler conditions with static single or paired paracrine stimuli that

99   induce fibroblast phenotypes that mimic specific phases of post-MI healing. Virtual

100   overexpression screens predicted both context-independent drivers of collagen synthesis

101   as well as regulators that differentially affect collagen expression in the context of

102   specific paracrine stimuli or phases of post-MI wound healing. Further model simulations

103   generated experimentally testable mechanistic hypotheses for the signaling underlying

104   such context-dependent responses, highlighting the utility of this computational model

105   for interrogating the complex roles of fibroblasts in the post-MI wound healing

106   environment.

107

Methods

Updates to Network Model of Fibroblast Signaling

110   We extended a large-scale computational model of fibroblast signaling [23] to be more

111   relevant for subsequent experimental study of fibroblast phenotype dynamics *in vivo*. As

112   described in previous studies[22, 50], the signaling model was implemented as a system

113   of logic-based differential equations with default normalized reaction and node

114   parameters. Here, the input nodes were separated from their associated ligand, and

115   outputs associated with collagen maturation (e.g. LOX) and myofibroblast differentiation

116   (e.g. contraction) were added[24–31]. See **Supplementary Methods** for more details. A

117   schematic of the network model highlighting the added interactions and nodes is shown

118   in **Figure S1**.

119

120   *Modeling the Dynamics of Post-MI Signaling and Collagen Expression*

121   To simulate a post-MI setting, we fit idealized time-dependent curves to experimental

122   timecourse data for the paracrine signals that act as inputs to the signaling model: IL1,

123   IL6, tumor necrosis factor α (TNFα), angiotensin II (AngII), endothelin-1 (ET1), TGFβ,

124   norepinephrine (NE), platelet-derived growth factor (PDGF), brain natriuretic peptide

125   (BNP; corresponding node in the model is natriuretic peptide or NP). In the logic-based

126   network model, inputs and signaling nodes are normalized to a continuous range from 0

127   to 1, where 1 represents a maximal level. The mechanical input was maintained at a

128   normalized level of 0.6 throughout the post-MI simulation, because mechanical strain

129   remains constant throughout the infarct healing timecourse in rats [32, 33]. Idealized

130   time-dependent multi-exponential curves ranging from normalized levels of 0.1 to 0.6

131   were fit to timecoursedata from previous studies [34–41] (see **Supplementary Methods**).

132   Due to a lack of available post-MI time course data from rat infarct zone alone, where

133   needed, we incorporated studies that measured these paracrine factors in rat whole heart

134   or border zone, or human serum post-MI (see **Table S1**).

135　　　　　To predict how single-cell changes in collagen expression lead to tissue-level

136　　　changes in percent collagen area fraction, we adapted a previously published model of

137　　　tissue-level collagen accumulation dynamics[42] and coupled it to the signaling model

138　　　described above. The tissue-level model integrates time-dependent MMP activity and

139　　　fibroblast numbers derived from previous studies of rat infarcts, as well as the collagen I

140　　　and III mRNA levels predicted by the signaling model (**Figure S2**). MMP activity is

141　　　approximated as a time-dependent function based on data from rat or mouse infarcts [43–

142　　　46] rather than being defined by predictions from the signaling model, because MMPs are

143　　　expressed by many cell types post-MI and fibroblast-specific expression does not fully

144　　　account for cardiac MMP levels[47]. The timecourse of fibroblast numbers was also

145　　　based on experimental data from rat infarcts[11]. This model is described in more detail

146　　　in the **Supplementary Methods**.

147　　　　　We validated model predictions of post-MI collagen I and III mRNA dynamics

148　　　against independent experimental data collected in rat infarcts [37, 48], in order to be

149　　　consistent with the species used to develop the model and input curves (rat or human

150　　　data). The predictions from the tissue-level model were validated against the collagen

151　　　area fraction measured in rat infarcts [49].

152

153　　*Modeling the Response to Static Paracrine Stimuli and Comparison with post-MI*

154　　*Dynamics*

155　　A constant stimulus of each single paracrine input and each input pair was set to a

156　　normalized level of 0.6, and the simulation was run to steady state. Steady-state

157   predictions in response to static paracrine stimuli were compared to predictions at

158   specific timepoints from the dynamic post-MI simulations (0 days, 1 day, 7 days, and 42

159   days) that correspond to different phases of infarct healing (pre-infarct, inflammatory,

160   proliferative, and maturing respectively). We used principal component analysis (*pca*

161   function in MATLAB) on mean-centered columns to compare static simulations and

162   specific time points from the dynamic simulations based on output profiles that

163   characterize the fibroblast phenotype (MMPs, collagens, other ECM proteins,

164   proliferation, contraction, and αSMA). The single- and paired-paracrine static simulations

165   that most closely matched the time points of interest from the dynamic post-MI

166   simulation were identified by calculating their Euclidean distance within the space

167   defined by the first three principal components.

168

169   *Screen for Intracellular Modulators of Collagen Expression*

170   To identify modulators of collagen expression, we individually simulated overexpression

171   of each node in the network and quantified its effect on the collagen expression nodes.

172   These comprehensive screens were performed under conditions with static pairs of

173   paracrine inputs representative of the different phases of post-MI healing, as well as with

174   the time-dependent post-MI simulation that include nine dynamic paracrine stimuli.

175   Overexpression of a given network node was simulated by increasing its normalized

176   expression parameter (ymax) 10-fold. Change in collagen expression (the sum of activity

177   from collagen I mRNA and collagen III mRNA) with overexpression (ymax = 10) was

178   expressed as the difference from a simulation with no overexpression (ymax = 1) at the

179   same timepoint and with the same paracrine stimuli.

180

Results

Expanding a fibroblast signaling network model to predict post-MI fibroblast

phenotype dynamics

A published large-scale computational model of cardiac fibroblast signaling [23] was

extended to make it more suited to predict the dynamics of fibroblast phenotype *in vivo*

(see **Methods** and **Figure S1**). While the signaling model was originally developed and

validated using a wealth of *in vitro* experimental data [23], we hypothesized that this

model could be extended to predict post-MI fibroblast dynamics because it is capable of

predicting semi-quantitative time-dependent behavior and it incorporates many of the

pathways involved in infarct healing (e.g. IL1, IL6, TGFβ, AngII). Thus, we coupled the

fibroblast network model with experimentally-based dynamic post-MI paracrine stimuli

and a tissue-level model of collagen accumulation (**Figure 1A**).

Timecourses for the nine paracrine model inputs were fit to multi-exponential

curves based on published experimental data from rat or human following myocardial

infarction (**Figure 1B**). Post-MI paracrine stimuli exhibited a range of distinct dynamic

behaviors, including rapid transients (IL6), slower transients (e.g. TGFβ, PDGF), and

rapid transients followed by a distinct slower phase (e.g. IL1, NE).

When driven by dynamic post-MI paracrine stimuli, the model predicts a wide

range of distinct time-dependent network responses (**Figure S3**) due to the distinct

behaviors of individual stimuli as well as pathway crosstalk and intra-network dynamics

(**Figure S4** and **Video S1**). The model predicts transient collagen I and III mRNA

202   expression dynamics that are similar to those observed in independent experimental data

203   from rat infarcts (**Figure 2A**)[37, 48]. Further, the coupled network and tissue models

204   predicted changes in collagen area fraction consistent with those measured in rat infarcts

205   (**Figure 2B**)[32].

206

207   **Relationship between fibroblast phenotypes induced by dynamic post-MI vs. static**

208   **paracrine stimuli**

209   *In vitro* experiments can provide precise control of simplified environmental conditions,

210   but it is unclear to what extent such conditions can reproduce the phenotype of fibroblasts

211   during the more dynamic and complex process of infarct healing[52]. Therefore, we used

212   the model to identify individual or pairs of static paracrine stimuli that drive phenotypes

213   that best mimic distinct phases of the post-MI fibroblast phenotype. The fibroblast model

214   was run to steady-state under stimulation with static levels of the nine paracrine stimuli as

215   well as all pairwise combinations (**Figure S5**). Using principal component analysis, we

216   visualized the phenotypic relationship between fibroblasts stimulated by these 45 static

217   paracrine conditions and the post-MI fibroblast phenotype timecourse (**Figure 3**). Of

218   note, TGFβ stimulation had a very distinct effect on fibroblast phenotype, correlating

219   with node loadings of pro-fibrotic outputs such as periostin, collagens, and αSMA near

220   the negative PC2 axis of **Figure 3A** and **Figure 3B**. In contrast, the node loadings for

221   MMP1/MMP14/proliferation and MMP2/MMP9 groups did not strongly associate with

222   any single stimulus.

10

223   We next examined the extent to which stimulation with one or two static

224   paracrine factors mimicked fibroblast phenotypes at specific times post-MI. Such

225   analysis can identify paracrine signals that drive specific phases of the post-MI fibroblast

226   phenotype. The inflammatory phase (1 day post-MI) was fairly well mimicked by static

227   IL1 (**Figure 3A**), which predicted proliferation, EDAFN, MMP1, and MMP14

228   expression but insufficient MMP2 or MMP9 expression (**Figure 3C**). The combination of

229   IL1+NE improved predictions only slightly. In contrast, the period we defined as

230   proliferative signaling at 7 days post-MI was not well mimicked by any single stimulus

231   (**Figure 3A**), highlighting the signaling complexity of this phase (**Figure S3** and **Figure**

232   **S4**). TGFβ mimicked aspects of the 7 day post-MI fibroblast phenotype (e.g. expression

233   of collagens I/III, αSMA, periostin), consistent with previous studies showing that mouse

234   fibroblasts at intermediate stages of post-MI healing are most similar to fibroblasts

235   stimulated by TGFβ [52]. However, TGFβ was predicted to be insufficient to fully mimic

236   the post-MI expression of multiple MMPs, proliferation, LOX, and collagen fiber cross-

237   linking. Combination of TGFβ with AngII significantly improved predictions of MMP

238   activity and fibroblast proliferation (**Figure 3C**). The late (42 day) time point was closely

239   associated with AngII or the combination of NP+AngII, which mimicked sustained

240   proliferation and expression of MMP1/MMP14. The paracrine pairs that induced

241   phenotypes most similar to post-MI day 1, 7, and 42 fibroblasts are consistent with their

242   elevation at those times post-MI as shown in **Figure 1**. Overall, these model predictions

243   indicate that early and late stages of the post-MI fibroblast phenotype are more readily

244   mimicked using single static stimuli, but intermediate post-MI timepoints involve many

11

245   interacting stimuli and a complex network state that is more challenging to mimic *in*

246   *vitro*.

247

248   **Predicting post-MI phase-specific regulators of fibroblast phenotype**

249   Identification of regulators that drive distinct fibroblast phenotypes would provide

250   a better understanding of the complex transitions that occur *in vivo* and may lead to

251   potential phase-targeted therapeutics with reduced side effects. We simulated a virtual

252   screen for regulators of collagen I/III mRNA expression by overexpressing each node in

253   the context of paired paracrine static stimuli that best mimic the inflammatory (IL1+NE)

254   or proliferative (TGFβ+AngII) post-MI phases, as well control conditions representative

255   of the pre-infarct environment (**Figure 4**). For each node, overexpression was simulated

256   by increasing that node's normalized expression parameter 10-fold. Several nodes such as

257   β1 integrin pathway members, ET1 pathway members, and MAP kinases like JNK were

258   predicted to drive collagen expression across all three paracrine contexts.

259   The overexpression screen also identified a number of context-specific regulators

260   of collagen expression. In the TGFβ+AngII stimulated condition, overexpression of

261   TGFβ or AngII pathway members such as Smad3, ERK, or NOX enhanced collagen

262   mRNA expression, while Smad7 and NP overexpression suppressed collagen mRNA.

263   However, overexpression of these nodes did not significantly affect collagen mRNA

264   expression in control or IL1+NE contexts. Overexpression of the "input IL1" node

265   moderately increased collagen expression under control or IL1+NE stimulation but

266   decreased collagen expression in the TGFβ+AngII context. This effect was dose-

267   dependent, as overexpression of the "IL1" node itself did not sufficiently stimulate the

268   IL1 receptor in the control and TGFβ+AngII conditions.

269   As static paracrine stimuli only partially mimic the history-dependent effect of the

270   dynamic post-MI paracrine environment (**Figure 3**), it is unknown to what extent

271   intracellular regulators of fibroblast phenotype identified under simplified conditions *in*

272   *vitro* can explain their role *in vivo*. To identify post-MI phase-specific regulators, we

273   performed a virtual overexpression screen of the 106 network nodes in the context of the

274   nine dynamic post-MI paracrine stimuli. Activity timecourses for each of the

275   overexpressed nodes in each of these 106 simulations are shown in **Figure S6**. Node

276   overexpression induced a diverse range of phase-specific effects on the post-MI

277   timecourses of collagen I/III mRNA expression (**Figure 5**). Overexpression of some

278   nodes was predicted to induce sustained collagen mRNA expression even before MI,

279   such as TGFβ, ETAR, JNK, and β1-integrin pathway members. These context-

280   independent nodes had an effect on collagen expression similar to that identified under

281   static control conditions (**Figure 4**). In contrast, several regulators strongly increased

282   (Smad3) or decreased (PKG) collagen mRNA only in the proliferative phase. Some

283   regulators such as NOX not only increased collagen mRNA in the proliferative phase but

284   sustained it into late phases. Other regulators had dichotomous effects, such as IL1,

285   which enhanced collagen mRNA during the inflammatory and late phases but decreased

286   collagen during the proliferative phase. Conversely, NFκB, IL6 and Akt overexpression

287   modestly suppressed early and late collagen mRNA expression but enhanced collagen

288   mRNA expression at intermediate timepoints.

289   **Mechanisms contributing to post-MI phase-specific regulation of collagen**

290   The mechanistic nature of the computational model enables identification of the specific

291   conditions and network mechanisms that underlie phase-specific regulation of collagen

292   expression. For specific influential nodes of interest, we performed additional simulations

293   representing different levels of overexpression or knockdown using the dynamic post-MI

294   model. We used the model's mechanistic network structure along with sensitivity

295   analysis as described previously [23] (data not shown) to identify simplified network

296   mechanisms that mediate the effects of these notable regulators of collagen expression.

297   For example, the model predicted that overexpression of Smad7 amplifies its activity and

298   decreases collagen mRNA expression only in the proliferative phase (1-2 weeks),

299   resulting in decreased collagen area fraction in the infarct throughout post-MI remodeling

300   (**Figure 6A**). This prediction is consistent with in vitro studies showing Smad7

301   overexpression decreases collagen expression in vitro[53], as well as our simulations of

302   the simplified AngII+TGFβ context (**Figure 3**).

303   Like Smad7, PKG was predicted to reduce collagen expression by inhibiting

304   Smad3 activity during the proliferative phase. However, its inhibitory effect on collagen

305   mRNA was more sustained due its more prolonged stimulation by the upstream paracrine

306   NP (**Figure 6B**). Interestingly, PKG was not predicted as a negative regulator in the static

307   AngII+TGFβ context context (**Figure 4**), as the simplified AngII+TGFβ context lacked

308   the NP stimulation of PKG activity (**Figure S5**). In contrast to Smad7 and PKG, Smad3

309   overexpression strongly enhanced collagen mRNA in the proliferative phase with

310   subsequent and sustained increase in collagen area fraction (**Figure S7**).

311

312   NOX overexpression was predicted to induce sustained NOX activity beginning

313   in the proliferative phase post-MI, primarily due to activation of multiple positive

314   feedbacks by AP1-TGFβ, NOX1-AP1-TGFβ, and AP1-ET1. The predicted AP1-TGFβ

315   feedback involves both AP1-dependent transcription and MMP-induced activation of

316   latent TGFβ. Together, these feedbacks induced sustained collagen I/III mRNA

317   expression (**Figure 6C**). NOX also induced partial negative regulation of collagen

318   mRNA via an incoherent feedforward circuit involving AP1-driven expression of IL6 and

319   activation of Smad7. Overall, NOX overexpression induced a strong increase in collagen

320   area fraction after MI.

321   IL1 exhibited a complex post-MI phase- and dose-dependent regulation of

322   collagen expression. With moderate IL1 overexpression, collagen mRNA increased only

323   moderately post-MI in the proliferation phase, driven primarily by the AP1-TGFβ

324   positive feedback to produce a somewhat larger but stable infarct (**Figure 6D**). In

325   contrast, strong IL1 overexpression enhanced collagen mRNA in the inflammatory phase,

326   reduced collagen mRNA during the proliferative phase, and then subsequently provoked

327   sustained collagen mRNA expression. The model predicted that the IL1 pathway has

328   multiple mechanisms by which it negatively regulates collagen expression in the

329   proliferative phase including: NFκB stimulation of the IL6/Smad7 pathway, p38-

330   mediated inhibition of ERK, and inhibition of the TGFβ pathway through upregulation of

331   the decoy receptor BAMBI (BMP and activin membrane-bound inhibitor). However in

332   later phases, the sustained collagen mRNA expression was primarily driven by continued

333   activation of the AP1-TFGβ positive feedback loop, resulting in delayed but continually

334   elevating fibrosis post-MI (**Figure 6D**). IL1 knockdown was not predicted to

335   significantly alter post-MI collagen expression. These predictions are in line with studies

336   that have shown IL1 inhibition is most effective in limiting collagen expression post-MI

337   when levels of inflammatory cytokines are high[8].

338   Both moderate and strong overexpression of β1-integrin induced substantial fibrosis even

339   before MI, consistent with its effect across all simplified paracrine contexts (**Figure 4,**

340   **Figure S6**) and the continual mechanical stress in the beating heart. Moderate ET1AR

341   overexpression induced strong and sustained collagen expression beginning in the

342   inflammatory phase post-MI, while strong ET1AR overexpression induced fibrosis even

343   in baseline conditions (**Figure S7**).

344

345   **3.5 Discussion**

346   Cardiac fibroblasts are central mediators of wound healing and cardiac function

347   after myocardial infarction [16, 49, 54], yet the complexity of the dynamic in vivo

348   paracrine environment and the fibroblast intracellular signaling network hinders

349   therapeutic targeting [55]. Here, we extended a large-scale computational model of the

350   fibroblast signaling network to identify paracrine and intracellular drivers of extracellular

351   matrix synthesis in specific phases of post-infarct healing. By integrating experimentally-

352   based post-MI dynamics of nine paracrine stimuli, the model accurately predicted the

353   dynamics of collagen expression as validated against experimental data from rat infarcts.

354   The model was applied to screen for drivers of collagen expression in the context of static

355   paracrine stimuli representative of specific post-MI phases, as well as the more complex

356   dynamic post-MI paracrine environment. These virtual overexpression screens identified

16

357   post-MI phase-specific regulators such as PKG and Smad7, which suppress collagen

358   expression in the proliferative phase via inhibition of Smad3; NOX, which sustained

359   fibrosis in proliferative and late phases via AP1-TGFβ feedback; and IL1, which induced

360   alternating enhancement and suppression of collagen expression. This study highlights

361   how fibroblast signaling pathways coordinate to dynamically control matrix synthesis

362   during wound healing, and invites further investigation into therapeutics that target

363   fibroblasts at specific post-MI phases.

364

365   *Loci of control in the fibroblast signaling network*

366   The complex, concomitant dynamics of many signaling pathways during infarct

367   healing has made it difficult to experimentally identify the signaling mediators that drive

368   collagen production[52]. Computational modeling enabled a detailed mechanistic

369   investigation into the determinants of collagen production by integrating many sources of

370   experimental data into a single framework. For example, the model predicted that Smad7

371   overexpression decreases collagen expression during the proliferative phase is consistent

372   with previous studies that found decreased collagen expression in fibroblasts after

373   overexpressing Smad7 *in vitro* [56] or after AngII-induced cardiac remodeling in mice

374   [57]. The prediction that PKG overexpression reduces collagen expression post-MI is

375   consistent with a previous study showing that upstream NP decreases post-MI fibrosis

376   [58]. This literature-based fibroblast network model predicts that both Smad7 and PKG

377   affect collagen expression via mechanisms that inhibit Smad3 [53, 59]. It is well-

378   understood that TGFβ induces collagen production, but inhibiting TGFβ signaling before

379   or after an MI can decrease the necessary collagen deposition during wound healing and

380   increase the risk of cardiac dilation and mortality in rats[56]. Further, Smad3 knockdown

381   was predicted to decrease post-MI fibrosis, consistent with previous studies[60]. Overall,

382   these simulations indicate that Smad3 is a critical target for negative regulation of

383   collagen expression in cardiac fibroblasts, which could direct future studies into other

384   inhibitors of Smad3 activation as a way to modulate excessive fibrosis.

385   Inflammation has been extensively tested as a potential driver of cardiac fibrosis.

386   It has been shown that higher pre-infarct levels of inflammation, high post-infarct levels

387   of inflammatory mediators, and longer duration of inflammation are associated with an

388   increase in fibrosis and a decrease in cardiac function post-MI[6, 8, 55, 61]. However, the

389   use of broad anti-inflammatory treatments such as NSAIDs or corticosteroids as well as

390   therapies targeted to specific inflammatory mediators have been shown to worsen

391   outcomes rather than improve cardiac health post-MI[7, 13, 17, 55, 62–65]. Furthermore,

392   although IL1 receptor inhibitors (e.g. Anakinra) have been shown to decrease cardiac

393   fibrosis, they increase the risk of major cardiac events and heart failure long term[7, 63].

394   Sano et al recently showed that IL1 receptor inhibition attenuated post-MI fibrosis in

395   mice with a TET2 mutation that increased inflammation, but in control mice, IL1

396   inhibition had no effect on collagen area fraction[8]. This is consistent with our

397   prediction that strongly increasing IL1 signaling increases collagen synthesis long-term,

398   while decreasing IL1 did not affect collagen. The role of IL1 in simultaneously inducing

399   and attenuating TGFβ signaling has not been fully elucidated in the heart. *In vitro* studies

400   of the effect of IL1 on fibroblast phenotype have not been fully consistent, highlighting

401   the fact that IL1 might have a very context-specific role. We identified three mechanisms

402   by which IL1 can attenuate TGFβ-induced collagen expression: the IL6 pathway, p38

18

403   signaling, and BAMBI upregulation. Examination of both bulk RNA-seq from fibroblasts

404   post-MI and single-cell RNA-seq from Wnt-expressing fibroblasts post-MI shows

405   increased expression of BAMBI in the proliferative phase [19, 66]. Further, BAMBI

406   knockout enhanced profibrotic responses in TGFβ-stimulated cardiac fibroblasts or after

407   transverse aortic constriction *in vivo* [67].

408   The model also predicted that NOX overexpression would increase collagen,

409   while NOX knockdown would not affect collagen expression. However, decreasing NOX

410   activity was previously shown to attenuate collagen expression post-MI[68]. This

411   discrepancy between the model predictions and *in vivo* data is likely due to the model not

412   predicting sufficient NOX activity post-MI without overexpression. NOX is downstream

413   of TGFβ, ET1, and AngII, which both our model predictions and previous experiments

414   demonstrate to enhance cardiac fibrosis[69, 70]. In the model, the mechanism by which

415   both NOX and IL1 overexpression increase collagen expression is via an AP1-TGFβ

416   positive feedback pathway. This predicted feedback loop is consistent with our previous

417   modeling of mechano-activated fibroblasts validated in collagen gels, previous studies

418   with lung fibroblasts, and in vivo studies demonstrating the critical role of AP1

419   component c-Jun in many fibrotic diseases[23, 71, 72]. Thus the role of AP1-TGFβ

420   positive feedback could be the focus of further studies into potential anti-fibrotic

421   therapies.

422

423   *The dynamic model as a tool for investigating wound healing*

424   There is a need for computational tools for investigation of wound healing in

425   order to more fully understand the development of fibrosis and identify potential

426   therapeutic strategies against it[20]. In the heart, early collagen production is important

427   for generating a strong scar[73], but continued production and fibrosis contribute to

428   diastolic dysfunction[1, 16, 74]. It has been shown that the timing of collagen production

429   is important in determining the ultimate health of the heart[64].

430   The dynamic modeling approach outlined in this study allowed for a direct

431   comparison between specific signaling pathways and the phases of fibroblast phenotype,

432   and this could be a tool for further investigation into cardiac fibrosis. We identified

433   representative stimuli that mimic fibroblast activity in the pre-infarct (control),

434   inflammatory (IL1+NE), proliferative (TGFB+AngII), and mature (NP+AngII) phases of

435   wound healing. These stimuli can be used to design *in vitro* experiments mimic *in vivo*

436   fibroblast phenotypes characteristic of specific time points during infarct healing. Future

437   studies could investigate how changing the timing of these signals affect collagen

438   expression. The model could be used to test the effect of potential novel therapeutics on

439   fibroblast phenotype. The modeling of differential expression of nodes in the network

440   invites the possibility of integrating gene expression data to investigate potential genetic

441   causes of adverse wound healing that lead to heart failure, patient-specific variability, or

442   single-cell heterogeneity. Furthermore, the model includes explicit network mechanisms,

443   which guide *in vitro* experiments to validate promising collagen regulators identified in

444   this study.

445

446   *Limitations and future directions*

447   The main limitation of this study is that the model predicts post-MI contributions

448   of fibroblasts but not other cell types such as macrophage and cardiomyocytes can alter

20

449   cardiac remodeling. The tissue level model only indirectly accounts for the activity of

450   these cells in collagen degradation and expression. Of note, the tissue level model does

451   not account for changes in MMP expression by fibroblasts, as the tissue-level MMP

452   activity that drives collagen degradation is assumed to be largely due to inflammatory

453   cells. Furthermore, processes such as re-vascularization (which can improve infarct

454   healing) or further cardiomyocyte injury (which can re-start or prolong wound healing

455   and induce pathologic remodeling) are not captured by this model. As in many

456   experimental screens and our past modeling of in vivo hypertrophy, here we performed

457   virtual overexpression screens. This approach has advantages of testing whether

458   overexpression is sufficient to modulate fibroblast phenotype and is more readily

459   validated experimentally with transgenic mice or viral vectors. Future studies may more

460   systematically explore simulations of genetic knockouts or small molecule inhibitors.

461   However, this model is a useful step toward investigating additional details of fibroblast

462   signaling dynamics and intercellular cross-talk post-MI.

463   In this study, we demonstrate that by integrating multiple time-dependent

464   paracrine stimuli, the fibroblast network model can predict many features and regulators

465   of post-MI fibroblast signaling and matrix remodeling. These predictions should be

466   validated *in vivo*, but initial validations may be most practical *in vitro* with the static

467   paracrine stimuli that we identified to mimic post-MI phases. Further studies could test

468   how variations in the timing of input stimuli affect fibroblast activity or incorporate this

469   model into a multi-scale model that can predict the effect of cell-cell interactions between

470   macrophage and cardiomyocytes. Future studies will also be necessary to determine how

21

471   therapeutic modulation of collagen dynamics can be leveraged to optimally improve

472   cardiac remodeling and contractility after myocardial infarction.

473
474   **CRediT author statement**

475   Angela Zeigler: Conceptualization, Writing - Original Draft, Software, Formal Analysis;

476   Anders Nelson: Software, Formal Analysis; Anirudha Chandrabhatla: Software, Formal

477   Analysis; Olga Brazhkina: Formal Analysis; Jeffrey Holmes: Conceptualization, Writing-

478   Reviewing and Editing; Jeffrey Saucerman: Conceptualization, Writing- Reviewing and

479   Editing.

480   **Acknowledgements**

486   **Conflict**

487   The authors have declared that no conflict of interest exists.

488

489   **References:**

490   [1]   Beltrami CA, Finato N, Rocco M, et al. Structural basis of end-stage failure in ischemic

491   cardiomyopathy in humans. *Circulation*; 89: 151–163.

492   [2]   O'Gara PT, Kushner FG, Ascheim DD, et al. 2013 ACCF/AHA guideline for the

493   management of st-elevation myocardial infarction: Executive summary: A report of

494   the American college of cardiology foundation/american heart association task force

495   on practice guidelines. *J Am Coll Cardiol* 2013. Epub ahead of print 2013. DOI:

496   10.1016/j.jacc.2012.11.018.

497 [3] Schocken DD, Benjamin EJ, Fonarow GC, et al. Prevention of heart failure: A scientific

498   statement from the American Heart Association Councils on epidemiology and

499   prevention, clinical cardiology, cardiovascular nursing, and high blood pressure

500   research; Quality of Care and Outcomes Research Interdisc. *Circulation* 2008. Epub

501   ahead of print 2008. DOI: 10.1161/CIRCULATIONAHA.107.188965.

502 [4] Gottdiener JS, Arnold a M, Aurigemma GP, et al. Predictors of congestive heart failure

503   in the elderly: the Cardiovascular Health Study. *J Am Coll Cardiol*; 35: 1628–1637.

504 [5] He J, Ogden LG, Bazzano LA, et al. Risk factors for congestive heart failure in US men

505   and women: NHANES I epidemiologic follow-up study. *Arch Intern Med*; 161: 996–

506   1002.

507 [6] Orn S, Ueland T, Manhenke C, et al. Increased interleukin-1β levels are associated

508   with left ventricular hypertrophy and remodelling following acute ST segment

509   elevation myocardial infarction treated by primary percutaneous coronary

510   intervention. *J Intern Med*; 272: 267–276.

511 [7] Morton AC, Rothman AMK, Greenwood JP, et al. The effect of interleukin-1 receptor

512   antagonist therapy on markers of inflammation in non-ST elevation acute coronary

513   syndromes: The MRC-ILA Heart Study. *Eur Heart J* 2015. Epub ahead of print 2015.

514   DOI: 10.1093/eurheartj/ehu272.

515 [8] Sano S, Oshima K, Wang Y, et al. Tet2-Mediated Clonal Hematopoiesis Accelerates

516   Heart Failure Through a Mechanism Involving the IL-1β/NLRP3 Inflammasome. *J Am*

517   *Coll Cardiol* 2018. Epub ahead of print 2018. DOI: 10.1016/j.jacc.2017.12.037.

518 [9] Fishbein MC, Maclean D, Maroko PR. The histopathologic evolution of myocardial

519   infarction. *Chest*; 73: 843–849.

520   [10]   Palatinus JA, Rhett JM, Gourdie RG. Translational lessons from scarless healing of

521   cutaneous wounds and regenerative repair of the myocardium. *Journal of Molecular*

522   *and Cellular Cardiology*; 48: 550–557.

523   [11]   Virag JI, Murry CE. Myofibroblast and Endothelial Cell Proliferation during Murine

524   Myocardial Infarct Repair. *Am J Pathol*; 163: 2433–2440.

525   [12]   Chistiakov DA, Orekhov AN, Bobryshev Y V. The role of cardiac fibroblasts in post-

526   myocardial heart tissue repair. *Experimental and Molecular Pathology*; 101: 231–240.

527   [13]   Hwang MW, Matsumori A, Furukawa Y, et al. Neutralization of interleukin-1beta in

528   the acute phase of myocardial infarction promotes the progression of left ventricular

529   remodeling. *J Am Coll Cardiol*; 38: 1546–53.

530   [14]   Volders PG, Willems IE, Cleutjens JP, et al. Interstitial collagen is increased in the non-

531   infarcted human myocardium after myocardial infarction. *J Mol Cell Cardiol*; 25:

532   1317–23.

533   [15]   Litwin SE, Litwin CM, Raya TE, et al. Contractility and stiffness of noninfarcted

534   myocardium after coronary ligation in rats. Effects of chronic angiotensin converting

535   enzyme inhibition. *Circulation*; 83: 1028–1037.

536   [16]   Turner NA, Porter KE. Function and fate of myofibroblasts after myocardial

537   infarction. *Fibrogenesis Tissue Repair*; 6: 5.

538   [17]   Pfeffer MA, Braunwald E. Ventricular remodeling after myocardial infarction.

539   Experimental observations and clinical implications. *Circulation*; 81: 1161–1172.

540   [18]   Sun Y, Weber KT. Infarct scar: A dynamic tissue. *Cardiovascular Research*; 46: 250–

541   256.

542   [19]   Mouton AJ, Ma Y, Rivera Gonzalez OJ, et al. Fibroblast polarization over the

543   myocardial infarction time continuum shifts roles from inflammation to

544 angiogenesis. *Basic Res Cardiol* 2019. Epub ahead of print 2019. DOI:

545 10.1007/s00395-019-0715-4.

546 [20] Ma Y, Iyer RP, Jung M, et al. Cardiac Fibroblast Activation Post-Myocardial Infarction:

547 Current Knowledge Gaps. *Trends in Pharmacological Sciences* 2017. Epub ahead of

548 print 2017. DOI: 10.1016/j.tips.2017.03.001.

549 [21] Jin Y-F, Han H-C, Berger J, et al. Combining experimental and mathematical modeling

550 to reveal mechanisms of macrophage-dependent left ventricular remodeling. *BMC*

551 *Syst Biol*; 5: 60.

552 [22] Zeigler AC, Richardson WJ, Holmes JW, et al. Computational modeling of cardiac

553 fibroblasts and fibrosis. *J Mol Cell Cardiol*. Epub ahead of print 19 November 2015.

554 DOI: 10.1016/j.yjmcc.2015.11.020.

555 [23] Zeigler AC, Richardson WJ, Holmes JW, et al. A computational model of cardiac

556 fibroblast signaling predicts context-dependent drivers of myofibroblast

557 differentiation. *J Mol Cell Cardiol*; 94: 72–81.

558 [24] López B, Querejeta R, González A, et al. Impact of treatment on myocardial lysyl

559 oxidase expression and collagen Cross-linking in patients with heart failure.

560 *Hypertension*; 53: 236–242.

561 [25] Voloshenyuk TG, Hart AD, Khoutorova E, et al. TNF-?? increases cardiac fibroblast

562 lysyl oxidase expression through TGF-?? and PI3Kinase signaling pathways. *Biochem*

563 *Biophys Res Commun*; 413: 370–375.

564 [26] Voloshenyuk TG, Landesman ES, Khoutorova E, et al. Induction of cardiac fibroblast

565 lysyl oxidase by TGF-β1 requires PI3K/Akt, Smad3, and MAPK signaling. *Cytokine*;

566 55: 90–97.

567 [27] Cox TR, Bird D, Baker AM, et al. LOX-mediated collagen crosslinking is responsible for

568 fibrosis-enhanced metastasis. *Cancer Res*; 73: 1721–1732.

569 [28] Yuan W, Varga J. Transforming growth factor-beta repression of matrix

570 metalloproteinase-1 in dermal fibroblasts involves Smad3. *J Biol Chem*; 276: 38502–

571 10.

572 [29] Hall MC, Young DA, Waters JG, et al. The comparative role of activator protein 1 and

573 Smad factors in the regulation of Timp-1 and MMP-1 gene expression by

574 transforming growth factor-β1. *J Biol Chem*; 278: 10304–10313.

575 [30] Hinz B, Celetta G, Tomasek JJ, et al. Alpha-smooth muscle actin expression

576 upregulates fibroblast contractile activity. *Mol Biol Cell* 2001. Epub ahead of print

577 2001. DOI: 10.1091/mbc.12.9.2730.

578 [31] Huet E, Vallée B, Szul D, et al. Extracellular matrix metalloproteinase inducer/CD147

579 promotes myofibroblast differentiation by inducing α-smooth muscle actin

580 expression and collagen gel contraction: Implications in tissue remodeling. *FASEB J*

581 2008. Epub ahead of print 2008. DOI: 10.1096/fj.07-8748com.

582 [32] Fomovsky GM, Rouillard AD, Holmes JW. Regional mechanics determine collagen

583 fiber structure in healing myocardial infarcts. *J Mol Cell Cardiol*; 52: 1083–90.

584 [33] Richardson WJ, Clarke SA, Alexander Quinn T, et al. Physiological implications of

585 myocardial scar structure. *Compr Physiol* 2015. Epub ahead of print 2015. DOI:

586 10.1002/cphy.c140067.

587 [34] White M, Rouleau JL, Hall C, et al. Changes in vasoconstrictive hormones, natriuretic

588 peptides, and left ventricular remodeling soon after anterior myocardial infarction.

589 *Am Heart J*; 142: 1056–1064.

590 [35] Schieffer B, Wirger A, Meybrunn M, et al. Comparative effects of chronic angiotensin-

591 converting enzyme inhibition and angiotensin II type 1 receptor blockade on cardiac

592 remodeling after myocardial infarction in the rat. *Circulation* 1994. Epub ahead of

593 print 1994. DOI: 10.1161/01.CIR.89.5.2273.

594 [36] Herskowitz a, Choi S, Ansari a a, et al. Cytokine mRNA expression in

595   postischemic/reperfused myocardium. *Am J Pathol*; 146: 419–428.

596 [37] Deten A, Hölzl A, Leicht M, et al. Changes in extracellular matrix and in transforming

597   growth factor beta isoforms after coronary artery ligation in rats. *J Mol Cell Cardiol*;

598   33: 1191–207.

599 [38] Hao J, Ju H, Zhao S, et al. Elevation of expression of Smads 2, 3, and 4, decorin and

600   TGF-β in the chronic phase of myocardial infarct scar healing. *J Mol Cell Cardiol* 1999.

601   Epub ahead of print 1999. DOI: 10.1006/jmcc.1998.0902.

602 [39] Deten A, Volz HC, Briest W, et al. Cardiac cytokine expression is upregulated in the

603   acute phase after myocardial infarction. Experimental studies in rats. *Cardiovasc Res*;

604   55: 329–340.

605 [40] Heba G, Krzemiński T, Porc M, et al. The time course of tumor necrosis factor-α,

606   inducible nitric oxide synthase and vascular endothelial growth factor expression in

607   an experimental model of chronic myocardial infarction in rats. *J Vasc Res* 2001. Epub

608   ahead of print 2001. DOI: 10.1159/000051057.

609 [41] Zhao W, Zhao T, Huang V, et al. Platelet-derived growth factor involvement in

610   myocardial remodeling following infarction. *J Mol Cell Cardiol* 2011. Epub ahead of

611   print 2011. DOI: 10.1016/j.yjmcc.2011.06.023.

612 [42] Richardson WJ, Clarke SA HJ. Modifying the Mechanics of Healing Infarcts: Better the

613   Enemy of Good? *J Mol Cell Cardiol* 2016.

614 [43] Carlyle WC, Jacobson AW, Judd DL, et al. Delayed reperfusion alters matrix

615   metalloproteinase activity and fibronectin mRNA expression in the infarct zone of

616   the ligated rat heart. *J Mol Cell Cardiol* 1997. Epub ahead of print 1997. DOI:

617   10.1006/jmcc.1997.0482.

618 [44] Cleutjens JPM, Kandala JC, Guarda E, et al. Regulation of collagen degradation in the

619   rat myocardium after infarction. *J Mol Cell Cardiol* 1995. Epub ahead of print 1995.

620   DOI: 10.1016/S0022-2828(05)82390-9.

621   [45] Peterson JT, Li H, Dillon L, et al. Evolution of matrix metalloprotease and tissue

622   inhibitor expression during heart failure progression in the infarcted rat. *Cardiovasc*

623   *Res* 2000. Epub ahead of print 2000. DOI: 10.1016/S0008-6363(00)00029-8.

624   [46] Tao Z-Y, Cavasin M a, Yang F, et al. Temporal changes in matrix metalloproteinase

625   expression and inflammatory response associated with cardiac rupture after

626   myocardial infarction in mice. *Life Sci*; 74: 1561–1572.

627   [47] Lindsey ML. Assigning matrix metalloproteinase roles in ischaemic cardiac

628   remodelling. *Nature Reviews Cardiology* 2018. Epub ahead of print 2018. DOI:

629   10.1038/s41569-018-0022-z.

630   [48] Zimmerman SD, Thomas DP, Velleman SG, et al. Time course of collagen and decorin

631   changes in rat cardiac and skeletal muscle post-MI. *Am J Physiol Heart Circ Physiol*;

632   281: H1816-22.

633   [49] Fomovsky GM, Holmes JW. Evolution of scar structure, mechanics, and ventricular

634   function after myocardial infarction in the rat. *Am J Physiol Heart Circ Physiol*; 298:

635   H221-8.

636   [50] Kraeutler MJ, Soltis AR, Saucerman JJ. Modeling cardiac β-adrenergic signaling with

637   normalized-Hill differential equations: comparison with a biochemical model. *BMC*

638   *Syst Biol*; 4: 157.

639   [51] White M, Rouleau JL, Hall C, et al. Changes in vasoconstrictive hormones, natriuretic

640   peptides, and left ventricular remodeling soon after anterior myocardial infarction.

641   *Am Heart J*; 142: 1056–64.

642   [52] Squires CE, Escobar GP, Payne JF, et al. Altered fibroblast function following

643   myocardial infarction. *J Mol Cell Cardiol*; 39: 699–707.

644   [53]   Wang B, Hao J, Jones SC, et al. Decreased Smad 7 expression contributes to cardiac

645   fibrosis in the infarcted rat heart. *Am J Physiol - Hear Circ Physiol* 2002.

646   [54]   Sun Y. Myocardial repair/remodelling following infarction: Roles of local factors.

647   *Cardiovascular Research*; 81: 482–490.

648   [55]   Ong SB, Hernández-Reséndiz S, Crespo-Avilan GE, et al. Inflammation following acute

649   myocardial infarction: Multiple players, dynamic roles, and novel therapeutic

650   opportunities. *Pharmacology and Therapeutics* 2018. Epub ahead of print 2018. DOI:

651   10.1016/j.pharmthera.2018.01.001.

652   [56]   Frantz S, Hu K, Adamek A, et al. Transforming growth factor beta inhibition increases

653   mortality and left ventricular dilatation after myocardial infarction. *Basic Res Cardiol*;

654   103: 485–492.

655   [57]   Wei LH, Huang XR, Zhang Y, et al. Smad7 inhibits angiotensin II-induced hypertensive

656   cardiac remodelling. *Cardiovasc Res* 2013. Epub ahead of print 2013. DOI:

657   10.1093/cvr/cvt151.

658   [58]   Soeki T, Kishimoto I, Okumura H, et al. C-type natriuretic peptide, a novel antifibrotic

659   and antihypertrophic agent, prevents cardiac remodeling after myocardial infarction.

660   *J Am Coll Cardiol* 2005. Epub ahead of print 2005. DOI: 10.1016/j.jacc.2004.10.067.

661   [59]   Ikeuchi M, Tsutsui H, Shiomi T, et al. Inhibition of TGF-?? signaling exacerbates early

662   cardiac dysfunction but prevents late remodeling after infarction. *Cardiovasc Res*; 64:

663   526–535.

664   [60]   Bujak M, Ren G, Kweon HJ, et al. Essential role of Smad3 in infarct healing and in the

665   pathogenesis of cardiac remodeling. *Circulation* 2007. Epub ahead of print 2007. DOI:

666   10.1161/CIRCULATIONAHA.107.704197.

667   [61]   Ono K, Matsumori a, Shioi T, et al. Cytokine gene expression after myocardial

668   infarction in rat hearts: possible implication in left ventricular remodeling.

669   *Circulation*; 98: 149–156.

670   [62]   Abbate A, Kontos MC, Grizzard JD, et al. Interleukin-1 Blockade With Anakinra to

671   Prevent Adverse Cardiac Remodeling After Acute Myocardial Infarction (Virginia

672   Commonwealth University Anakinra Remodeling Trial [VCU-ART] Pilot Study). *Am J*

673   *Cardiol* 2010. Epub ahead of print 2010. DOI: 10.1016/j.amjcard.2009.12.059.

674   [63]   Abbate A, Van Tassell BW, Biondi-Zoccai G, et al. Effects of interleukin-1 blockade

675   with anakinra on adverse cardiac remodeling and heart failure after acute

676   myocardial infarction [from the virginia commonwealth university-anakinra

677   remodeling trial (2) (vcu-art2) pilot study]. *Am J Cardiol* 2013. Epub ahead of print

678   2013. DOI: 10.1016/j.amjcard.2013.01.287.

679   [64]   Garcia RA, Go K V., Villarreal FJ. Effects of timed administration of doxycycline or

680   methylprednisolone on post-myocardial infarction inflammation and left ventricular

681   remodeling in the rat heart. *Mol Cell Biochem* 2007. Epub ahead of print 2007. DOI:

682   10.1007/s11010-006-9379-0.

683   [65]   Kirlin PC, Romson JL, Pitt B, et al. Ibuprofen-mediated infarct size reduction: Effects

684   on regional myocardial function in canine myocardial infarction. *Am J Cardiol* 1982.

685   Epub ahead of print 1982. DOI: 10.1016/0002-9149(82)91244-9.

686   [66]   Farbehi N, Patrick R, Dorison A, et al. Single-cell expression profiling reveals dynamic

687   flux of cardiac stromal, vascular and immune cells in health and injury. *Elife* 2019.

688   Epub ahead of print 2019. DOI: 10.7554/eLife.43882.

689   [67]   Villar A V., García R, Llano M, et al. BAMBI (BMP and activin membrane-bound

690   inhibitor) protects the murine heart from pressure-overload biomechanical stress by

691   restraining TGF-β signaling. *Biochim Biophys Acta - Mol Basis Dis* 2013. Epub ahead of

692   print 2013. DOI: 10.1016/j.bbadis.2012.11.007.

693   [68]   Pan LL, Liu XH, Shen YQ, et al. Inhibition of NADPH oxidase 4-related signaling by

694   sodium hydrosulfide attenuates myocardial fibrotic response. *Int J Cardiol* 2013.

695   Epub ahead of print 2013. DOI: 10.1016/j.ijcard.2013.06.007.

696   [69] Xu J, Carretero OA, Lin CX, et al. Role of cardiac overexpression of ANG II in the

697   regulation of cardiac function and remodeling postmyocardial infarction. *Am J Physiol*

698   *- Hear Circ Physiol* 2007. Epub ahead of print 2007. DOI:

699   10.1152/ajpheart.00379.2007.

700   [70] Ammarguellat F, Larouche I, Schiffrin EL. Myocardial fibrosis in DOCA-salt

701   hypertensive rats: Effect of endothelin ETA receptor antagonism. *Circulation* 2001.

702   Epub ahead of print 2001. DOI: 10.1161/01.CIR.103.2.319.

703   [71] Sullivan DE, Ferris M, Nguyen H, et al. TNF-α induces TGF-β1 expression in lung

704   fibroblasts at the transcriptional level via AP-1 activation. *J Cell Mol Med* 2009. Epub

705   ahead of print 2009. DOI: 10.1111/j.1582-4934.2008.00647.x.

706   [72] Wernig G, Chen SY, Cui L, et al. Unifying mechanism for different fibrotic diseases.

707   *Proc Natl Acad Sci U S A* 2017. Epub ahead of print 2017. DOI:

708   10.1073/pnas.1621375114.

709   [73] Jugdutt BI, Joljart MJ, Khan MI. Rate of Collagen Deposition during Healing and

710   Ventricular Remodeling after Myocardial Infarction in Rat and Dog Models.

711   *Circulation* 1996. Epub ahead of print 1996. DOI: 10.1161/01.CIR.94.1.94.

712   [74] Weber KT, Sun Y, Bhattacharya SK, et al. Myofibroblast-mediated mechanisms of

713   pathological remodelling of the heart. *Nat Rev Cardiol*; 10: 15–26.

714

715

716 **Figure Legends**

717 **Figure 1: Computational model of post-MI fibroblast dynamics.** A) Schematic of coupled

718 model of post-MI fibroblast dynamics, incorporating dynamic paracrine stimuli, a fibroblast

719 signaling network, and tissue-level collagen metabolism. B) Dynamic paracrine stimuli were

720 modeled by fitting idealized multi-exponential curves to post-MI timecourse data from the

721 literature [35–39, 41, 51]. These time-dependent signals provide inputs to the signaling

722 network model. Experimental data were digitized from the indicated sources.

723 **Figure 2: Modeling of post-MI fibroblast signaling reproduces dynamics of post-MI**

724 **collagen expression and deposition.** A) Validation of the predicted timing of collagen

725 expression post MI against data from rat infarcts. B) Validation of predicted collagen

726 accumulation (area fraction) post-MI from the tissue-level model. Experimental data were

727 digitized from [37, 48].

728 **Figure 3: Simplified paracrine stimuli that mimic distinct phases of the post-MI fibroblast**

729 **phenotype.** A) Principal component analysis (PCA) to visualize the fibroblast phenotype at

730 specific times post-MI (red circles) or at steady state with 45 static paracrine conditions

731 (representative singles in dark blue, pairs in light blue). B) PCA node loadings show the

732 contribution of each node towards the overall predicted fibroblast phenotype in the first two

733 principal components. C) Activity profile of fibroblast phenotype nodes at selected timepoints

734 from dynamic post-MI simulations (left), or at steady-state with the best matching single (center)

735 or paired (right) paracrine stimuli.

736 **Figure 4: Modulators of collagen mRNA in the context of static paracrine stimuli that**

737 **mimic inflammatory (IL1+NP) and proliferative (TGFβ+AngII) phases.** Network nodes were

738 each overexpressed 10-fold (normalized expression parameter ymax = 10) in the context of the

739 indicated static paracrine stimuli (set to 0.6 normalized activity), predicting the change in

740 collagen I and III mRNA compared to no overexpression. Nodes were rank-ordered by their

741   predicted effect on collagen I and III mRNA expression with no paracrine stimulus (Control).

742   Smad3, PKG, NOX, IL1, ETAR and B1int are emphasized for comparison with subsequent

743   simulations of post-MI dynamics. Overexpressed nodes that did not affect collagen mRNA in any

744   condition are not shown

745   **Figure 5: Post-MI overexpression screen to identify phase-specific regulators of**
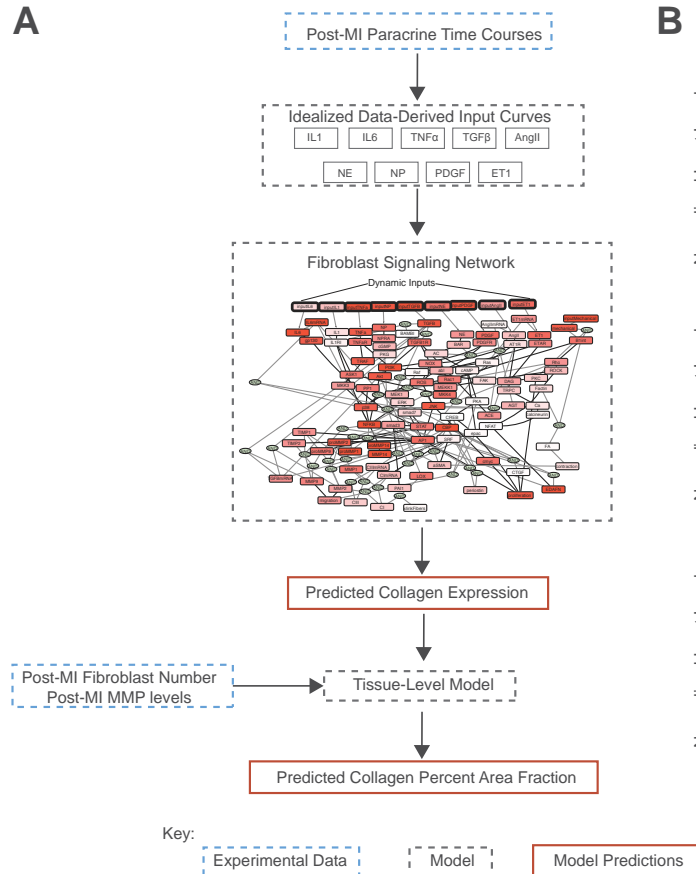
746   **collagen mRNA expression**. Each row shows the effect of 10-fold overexpression of the

747   indicated node. The predicted change in collagen expression is calculated as [Collagen I

748   mRNA + Collagen III mRNA]$_{overexpressed}$ - [Collagen I mRNA + Collagen III mRNA]$_{control}$.

749   Overexpressed nodes that did not affect collagen mRNA in any condition are not shown.
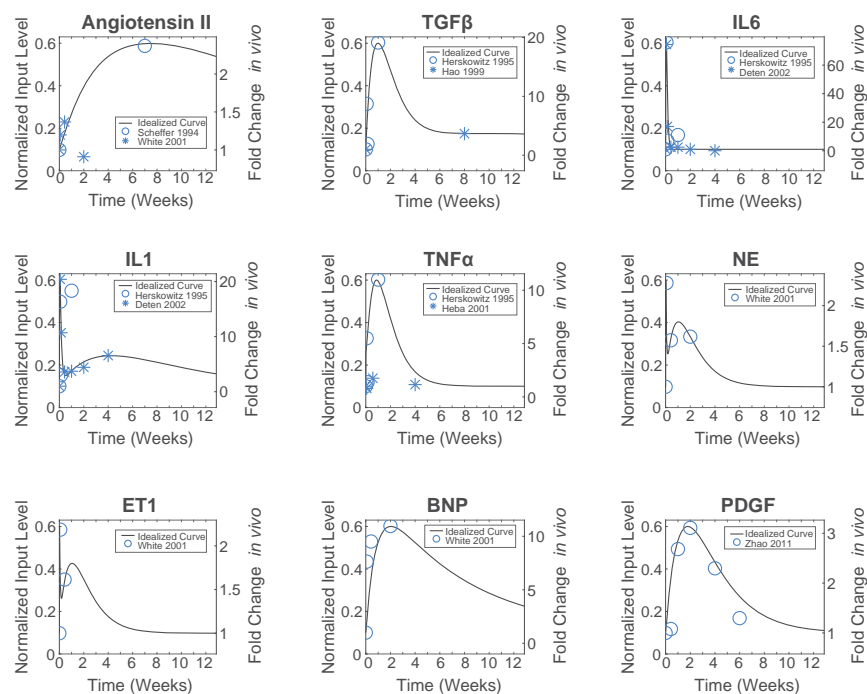
750   .**Figure 6: Mechanisms contributing to context-dependent regulators of collagen expression**

751   **post-MI.** Overexpression or knockdown were simulated by increasing or decreasing the

752   normalized expression parameter (ymax) for Smad7 (panel A), PKG (B), NOX (C), IL1 (D). The

753   resulting post-MI dynamics of that node's activity, collagen mRNA expression, and collagen area

754   fraction are shown. Simplified schematics indicate the network mechanisms by which these nodes
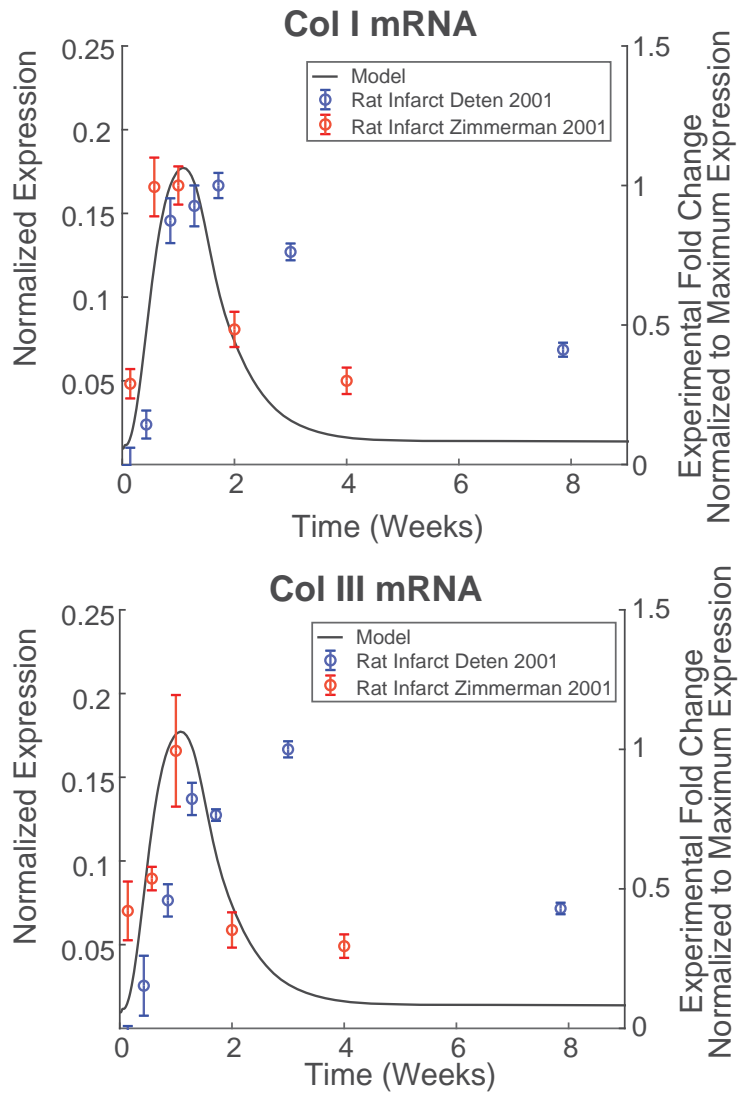
755   regulate collagen expression.

756

A

B

A PCA of Post-MI Dynamics and Static Stimuli

B Loadings of Nodes

C Dynamic Post-MI / Single Static / Paired Static